Vanishing artificial diffusion as a mechanism to accelerate convergence for multiphase porous media flow

P. Salinas[a,b,*], C. C. Pain[a,b], H. Osman[a,b], C. Jacquemyn[a,b], Z. Xie[c], M. D. Jackson[b]

[a] *Applied Modelling and Computation Group, Department of Earth Science and Engineering, Imperial College London, UK*
[b] *Novel Reservoir Modelling and Simulation Group, Department of Earth Science and Engineering, Imperial College London, UK*
[c] *Now at School of Engineering, Cardiff University, Cardiff, CF24 3AA, UK*

Abstract

Numerical solution of the equations governing multiphase porous media flow is challenging. A common approach to improve the performance of iterative non-linear solvers for these problems is to introduce artificial diffusion. Here, we present a mass conservative artificial diffusion that accelerates the non-linear solver but vanishes when the solution is converged. The vanishing artificial diffusion term is saturation dependent and is larger in regions of the solution domain where there are steep saturation gradients. The non-linear solver converges more slowly in these regions because of the highly non-linear nature of the solution. The new method provides accurate results while significantly reducing the number of iterations required by the non-linear solver. It is particularly valuable in reducing the computational cost of highly challenging numerical simulations, such as those where physical capillary pressure effects are dominant. Moreover, the method allows converged solutions to be obtained for Courant numbers that are at least two orders of magnitude larger than would otherwise be possible.

Keywords: Implicit formulation, Artificial diffusion;, Discontinuous Galerkin, Multiphase flows, Porous media

*Corresponding author.
Email address: pablo.salinas@imperial.ac.uk (P. Salinas)

1. Introduction

Modelling multiphase porous media flows is important in many subsurface reservoirs such as geothermal energy resources (Hilpert et al. (2016)), groundwater sources and deep saline aquifers (Janković et al. (2006)), geological CO_2 storage (Soltanian et al. (2016)), magma reservoirs (Solano et al. (2014)) and hydrocarbon reservoirs (Tchelepi et al. (2007)). However, numerical simulation of multiphase porous media flow is very challenging due to its highly non-linear nature. The non-linearities primarily arise from the saturation-dependence of relative permeability and capillary pressure (Jenny et al. (2009); Debbabi et al. (2017a), Debbabi et al. (2017b), McWhorter and Sunada (1990); Schmid and Geiger (2013); Kvashchuk (2015); Nooruddin and Blunt (2016)).

Controlling the non-linearities is essential to obtain stable solutions with Courant numbers that do not prohibitively increase the computational time. Many methods have been suggested: chopping of saturation based on heuristics (Jenny et al. (2009); Li and Tchelepi (2015b); Anderson (1965); Lott et al. (2012); Salinas et al. (2017a)), ordering-based non-linear solvers (Kwok and Tchelepi (2007); Natvig and Lie (2008); Hamon and Tchelepi (2016)), modified flux discretisation methods (Lee et al. (2015); Hamon et al. (2016)), continuation-Newton and parametrisation-based schemes (Younis et al. (2010); Brenner and Cances (2017); Jiang and Tchelepi (2018)) and phase field approaches (Cogswell and Szulczewski (2017)).

A common method to stabilise the system arising from the discretisation of the advection equation is to introduce artificial diffusion (Jameson (1995); Quarteroni and Valli (2009)). However, it can be challenging to find a balance such that the artificial diffusion accelerates convergence while not severely modifying the final result (Quarteroni and Valli (2009)).

In (Salinas et al. (2017a)) a vanishing artificial diffusion (VAD) was presented. The concept was to gradually reduce the amount of artifical diffusion as the solver converges, such that the artificial diffusion is small once convergence is achieved. The method allows the use of larger artificial diffusion, thus reducing the computational effort required for each non-linear solve, whilst minimising the effect of the artificial diffusion on the final result.

In (Salinas et al. (2017a)), the convergence of the non-linear solver was used to control the level of VAD by multiplying the artificial diffusion term by the difference between the most recent saturation estimation and the one obtained in the previous non-linear iteration. The method is very efficient;

however, it is not mass conservative, because the saturation estimation from the previous non-linear iteration is introduced in the right-hand side of the equations (Salinas et al. (2017a)), acting as a source/sink term for that specific phase.

Here, an improved, mass conservative VAD is presented. The new approach is based on two main concepts. First, VAD is introduced in all phases, which ensures that mass is conserved. Any residual VAD left after the non-linear solver converges behaves as a standard artificial diffusion. Second, the VAD is based on the local saturation value. In this way, the VAD is large in regions of the model domain where there are steep gradients in saturation and smaller elsewhere. These regions are typically where the non-linear solver converges more slowly because of the highly non-linear nature of the solution.

The modifications from the VAD presented in (Salinas et al. (2017a)) yield significant improvements. As we show here, the new formulation improves the stability and efficiency of the non-linear solver, reducing the number of non-linear iterations in all tested cases, irrespective of whether gravity and/or capillary pressure are present and in highly heterogeneous reservoir problems. The method is implemented and tested in a modified version of the fixed point method of Anderson (Anderson (1965); Salinas et al. (2017a)). However, it is a modification of the original continuum equations and should also work for implementation based on the Newton-Raphson method (Aziz and Settari (1979); Li and Tchelepi (2015a)).

The paper is organised as follows. The governing equations and numerical methods are presented in Section 2. The new VAD implementation is detailed in Section 3. The presented method is tested in a number of example cases, including comparison against analytical solutions in Section 4. Finally, some concluding remarks are presented in Section 5.

2. Governing equations

A summary of the equations is presented here; for details of the discretisation method used, see (Jackson et al. (2015); Gomes et al. (2017)). The multiphase Darcy's law for a phase α is given by:

$$\mathbf{q}_\alpha = \frac{\mathcal{K}_{r_\alpha}\mathbf{K}}{\mu_\alpha}\left(-\nabla p_\alpha + \rho_\alpha \mathbf{g}\right), \tag{1}$$

Considering a wetting and a non-wetting phase and including capillary pressure, Darcy's Law can be written in a slightly modified form as:

$$\mathbf{v}_w = \underline{\underline{\sigma}}_w \mathbf{u}_w = -\nabla p + \nabla p_c + \rho_w \mathbf{g}, \tag{2}$$

$$\mathbf{v}_{nw} = \underline{\underline{\sigma}}_{nw} \mathbf{u}_{nw} = -\nabla p + \rho_{nw} \mathbf{g}, \tag{3}$$

in which the subscripts w and nw stand for wetting and non-wetting phase respectively, $\mathbf{v}$ is the force density, $\mathbf{u}$ is the phase saturation-weighted Darcy velocity of phase, p and p_c are the pressure and the capillary pressure, respectively; ρ is the density of a phase, and $\underline{\underline{\sigma}}_\alpha$ (where α is either the wetting or the non-wetting phase) is defined as:

$$\underline{\underline{\sigma}}_\alpha = \mu_\alpha S_\alpha \left(\mathcal{K}_{r_\alpha} \mathbf{K}\right)^{-1}, \tag{4}$$

where $\mathcal{K}_{r_\alpha}$ is the relative permeability, μ_α the viscosity and S_α the saturation of phase α respectively and $\mathbf{K}$ is the permeability tensor.

The saturation equation for incompressible flow is:

$$\phi \frac{\partial S_\alpha}{\partial t} + \nabla \cdot (\mathbf{u}_\alpha S_\alpha) = s_{cty,\alpha}, \tag{5}$$

where s_{cty} is a source term and ϕ is the porosity.

The system of equations is closed by ensuring that the sum of the saturations is given by:

$$S_w + S_{nw} = 1. \tag{6}$$

The spatial discretisation considered in this paper is based on the Double Control Volume Finite Element method (described in detail in (Salinas et al. (2017b)), which is an improvement of the commonly used Control Volume Finite Element method (Forsyth (1991); Fung et al. (1992); Durlofsky (1993, 1994); Geiger et al. (2004); Wheeler and Yotov (2006); Matthai et al. (2007); Schmid et al. (2013); Jackson et al. (2015); Abushaikha et al. (2015); Mostaghimi et al. (2015); Xie et al. (2016); Abushaikha et al. (2017)). Here, the velocity is discretised using finite elements, but pressure and saturation are discretised using control volumes. This modification improves the quality of the pressure matrix for the large-angle elements often found in high-aspect ratio, subsurface reservoir problems (Deveugle et al. (2011); Jackson et al. (2015)). Solving the pressure matrix using the DCVFEM is faster than the classical approach and can also provide solutions for systems where the

classical approach fails. Moreover, pressure and saturation are consistently represented, as both use the same shape functions. Therefore, fields calculated from the saturation but resolved in the pressure space, such as capillary pressure and gravity effects, are in this way consistently represented.

Here, the element pair $P_{n-1}DGP_nCV$ is used. P_{n-1} stands for the order of discretisation of the velocity, DG stands for discontinuous Galerkin, P_n refers to the order of discretisation of the pressure and CV denotes the use of control volume shape functions. Note that the discretised velocity must be of one degree less than that of the pressure. Time is discretised using a Θ-method, where Θ smoothly varies between 0.5 (Crank-Nicolson) and 1 (implicit Euler) based on a total variation diminishing (TVD) criterion (Pavlidis et al. (2014)). This ensures that the method is unconditionally stable for any time-step size. Thus, the non-linear solver is the only factor limiting the stability of the solutions. The flux is calculated using a high order method with flux limiting to remove oscillations in saturation if required, as described in (Gomes et al. (2017)).

The non-linear solver is a modified fixed point method of Anderson detailed in (Salinas et al. (2017a)). It is a Picard iterative method, accelerated by the use of (i) backtracking, (ii) an internal iteration around the highly coupled solutions of velocity and saturation, (iii) a relaxation parameter based on the history of convergence, and (iv) use of previous guesses for solution fields; each of these methods increases the rate of convergence. Note that the VAD presented here is independent of the non-linear solver and spatial discretisation used and can be implemented in any method so long as the time discretisation is implicit.

The presented numerical methods reported here are implemented in the open-source code IC-FERST (Imperial College Finite Element Reservoir SimulaTor).

3. A mass conservative vanishing artificial diffusion

In (Salinas et al. (2017a)), an implememtation of VAD was presented to help reduce the non-linearity of the equations, mainly controlled by the saturation equation (Jenny et al. (2009)). The equation presented in (Salinas et al. (2017a)) to introduce the VAD is as follows:

$$\phi \frac{\partial S_{k\alpha}}{\partial t} + \nabla \cdot (\mathbf{u}_\alpha S_{k\alpha} - \kappa \nabla (S_{k\alpha} - S_{k'\alpha})) = s_{cty,\alpha}, \tag{7}$$

where κ is an over-relaxation term that controls the amount of artificial diffusion and k is the non-linear iteration. This equation was introduced only in one phase.

To introduce the new VAD term reported here, first Eq. 2 is modified by introducing $\nabla\kappa$:

$$\mathbf{v}_w = \underline{\underline{\sigma}}_w \mathbf{u}_w = -\nabla p + \nabla p_c + \nabla\kappa + \rho_w \mathbf{g}, \tag{8}$$

Note that this equation is not used when solving for pressure; rather, Eq. 2 is used. However, equation (9) is used to formulate a modified velocity that is then used in the mass conservation equation. The modified velocity is obtained by moving $\nabla\kappa$ to the left-hand-side:

$$\underline{\underline{\sigma}}_w \left(\mathbf{u}_w - \underline{\underline{\sigma}}_w^{-1} \nabla\kappa \right) = -\nabla p + \rho_w \mathbf{g}, \tag{9}$$

where terms between the brackets form the modified velocity. Substituting this in the saturation equation (Eq. 5) yields:

$$\phi \frac{\partial S_{kw}}{\partial t} + \nabla \cdot \left(S_{kw} (\mathbf{u}_w - \underline{\underline{\sigma}}_w^{-1} \nabla\kappa) \right) = s_{cty,w}. \tag{10}$$

Since κ depends on the saturation, the chain rule is applied to the $\nabla\kappa$ term, obtaining:

$$\phi \frac{\partial S_{kw}}{\partial t} + \nabla \cdot \left(S_{kw} (\mathbf{u}_w - \underline{\underline{\sigma}}_w^{-1} \frac{\partial \kappa}{\partial S_{kw}} \nabla S_{kw}) \right) = s_{cty,w}. \tag{11}$$

We now choose to modify the wetting phase equation to ensure mass conservation and create the VAD term. To this end, S_{kw} is substituted by the difference between non-linear iterations of the saturation, $(S_{k\alpha} - S_{k'\alpha})$, so the term vanishes as the saturation converges:

$$\phi \frac{\partial S_{kw}}{\partial t} + \nabla \cdot (S_{kw} \mathbf{u}_w) - 0.5 \nabla \cdot \left(S_{kw} \underline{\underline{\sigma}}_{kw}^{-1} \frac{\partial \kappa}{\partial S_{kw}} \nabla (S_{kw} - S_{k'w}) \right) = s_{cty,w}, \tag{12}$$

Next, to achieve mass conservation, we now also introduce the VAD term in the non-wetting phase equation. The term multiplying the gradient is the same for both phases (i.e. depends on the wetting phase), but the VAD term is specific to each phase:

$$\phi \frac{\partial S_{knw}}{\partial t} + \nabla \cdot (S_{knw} \mathbf{u}_{nw}) - 0.5 \nabla \cdot \left(S_{kw} \underline{\underline{\sigma}}_{kw}^{-1} \frac{\partial \kappa}{\partial S_{kw}} \nabla (S_{knw} - S_{k'nw}) \right) = s_{cty,nw}. \tag{13}$$

Note that only the saturation equations are modified; the remaining equations to be solved were defined in the previous section. By introducing the VAD term in the mass conservation equations for both phases, the source/sink terms balance, thus ensuring that mass is conserved. This can easily be proved by combining Eq. 13 with Eq. 6:

$$\phi\frac{\partial(1-S_{kw})}{\partial t}+\nabla\cdot((1-S_{kw})\mathbf{u}_{nw})+0.5\nabla\cdot\left(S_{kw}\underline{\underline{\sigma}}_{kw}^{-1}\frac{\partial\kappa}{\partial S_{kw}}\nabla(S_{kw}-S_{k'w})\right)=s_{cty,nw}, \tag{14}$$

which shows that the VAD term is the same as in Eq. 12 but with opposite sign. Therefore, we conserve the saturations S_{kw} and S_{knw} and, because the system is incompressible, the mass of each phase.

Similar to (Salinas et al. (2017a)), a Peclet-like number ($P_{sc}=\mathbf{v}_{w_i}l/\kappa$) is used to control the amount of VAD that is introduced; this is the parameter chosen by the user. To ensure that the VAD targets the most significant non-linearities (such as shock-fronts), the VAD model follows a capillary-pressure-like equation which is an exponential function of saturation and, for element i, the VAD to be introduced is calculated as:

$$\kappa_i=\frac{|v^*_{w_i}|\,l}{P_{sc}}\left(\frac{S_{w_i}-S_{wirr}}{1-S_{wirr}}\right)^{-n_\kappa}, \tag{15}$$

where l is the characteristic length of the domain, $v^*_{w_i}$ is the force density of the wetting phase of element i averaged over the dimensions (i.e. $v^*_{w_i}=\Sigma_{n=1}^{\mathcal{N}}|\mathbf{v}_{w_{ij}}|_n/\mathcal{N}$, where $\mathcal{N}$ are the number of dimensions), P_{sc} is the chosen Peclet-like number (user input parameter), n_κ is the saturation exponent, S_{w_i} is the saturation of the wetting phase for element i and S_{wirr} is the irreducible wetting phase saturation. The saturation term in brackets ensures that the VAD focuses on saturation gradients, while the term outside the brackets controls the magnitude of the VAD to be used.

The use of local κ_i is equivalent to having different materials with very different diffusion coefficients (potentially several orders of magnitude) throughout the domain, which affects the performance of the non-linear solver. Using a single value of κ throughout the domain provides better performance. The amount of VAD introduced is still local despite the use of uniform κ because the VAD also depends on the local difference in saturation between two non-linear iterations. It is preferable to use a local measure of convergence to control the local VAD as it is a better measure of the local performance of

the non-linear solver. Here, we choose to calculate the uniform κ as an average of the maximum and minimum values of κ_i throughout the domain at each time-level:

$$\kappa = 0.5(max(\kappa_i) - min(\kappa_i)). \tag{16}$$

In order to select the value of P_{sc} the user has to consider several issues. Higher values of VAD should further accelerate convergence of the non-linear solver; however, introducing very large VAD may cause the solution to deviate too far from the actual solution, such that the non-linear solver will have to backtrack more. Lower values of VAD may have little effect in reducing the non-linearities of the system, such that there will be no improvement in the convergence of the non-linear solver. As dicussed later, experience with the method suggests that suitable values yield initial VAD at least two orders of magnitude smaller than the viscous forces (i.e. $P_{sc} \geq 100$).

3.1. Effect of VAD on the flux

Here the stability of the introduced VAD is analysed considering its effect on the upwinding direction used to advect information. From Eq. 12 it can be seen that the flux across the boundary of a control volume is given by:

$$F_{ij} = \Gamma_{ij} S_{kw} (\mathbf{u}_{w_{ij}} - 0.5 \underline{\underline{\sigma}}^{-1}_{kw} \frac{\partial \kappa}{\partial S_{kw}} \nabla (S_{kw} - S_{k'w})), \tag{17}$$

where Γ_{ij} is the boundary between control volume i and j and F_{ij} is the flux across the boundary. Here, the upwinding direction is defined by $\mathbf{u}_{w_{ij}}$, so introducing an effective flux that does not follow this direction may yield non-monotonic saturation results.

It can be seen from Eq. 12 and 13, that for the VAD to completely vanish, the term $(S_{kw} - S_{k'w})$ has to be zero. However, it is very common to stop the non-linear solver before this limit is reached; a typical criterion for convergence might be when the infinitum norm of that difference is 0.01. Therefore, the VAD may not entirely disappear. If this happens, the VAD acts like a normal artificial diffusion term and, as discussed later, we have observed that the results may lose monotonicity when using high-order methods/elements to calculate the fluxes (as described in (Gomes et al. (2017))). In this case, a larger value of P_{sc} may be required or the convergence criterion may need to be decreased. When using first-order schemes, we have observed that the results are always monotonic.

3.2. Algorithm implementation

In the implementation reported here, the tensor $\underline{\underline{\sigma}}_{kw_{ij}}$ is projected onto the control volume interface and the saturation multiplying the vanishing term, κ and $\underline{\underline{\sigma}}_{kw_{ij}}$ is calculated using the values from the previous non-linear iteration, denoted using a prime, yielding:

$$\phi\frac{\partial S_{kw}}{\partial t}+\nabla\cdot(S_{kw}\mathbf{u}_w)-0.5\nabla\cdot\left(S_{k'w}\mathbf{n_{ij}}\cdot\underline{\underline{\sigma}}^{-1}_{k'w_{ij}}\cdot\mathbf{n_{ij}}\frac{\partial\kappa'}{\partial S_{kw}}\nabla(S_{kw}-S_{k'w})\right)=s_{cty,w}, \tag{18}$$

where $\mathbf{n_{ij}}$ is the outward pointing normal vector going from node i to node j. Substituting κ, from Eq. 15 and calculating $|v^*_{w_i}|$ using the values from the previous non-linear iteration, the final equation is:

$$\phi\frac{\partial S_{kw}}{\partial t}+\nabla\cdot(S_{kw}\mathbf{u}_w)+0.5\nabla\cdot\left(n_\kappa S_{k'w}\mathbf{n_{ij}}\cdot\underline{\underline{\sigma}}^{-1}_{k'w_{ij}}\cdot\mathbf{n_{ij}}\frac{|v^*_{w'_i}|\,l(S_{k'w_i}-S_{wirr})^{(-n_\kappa-1)}}{P_{sc}(1-S_{wirr})^{-n_\kappa}}\nabla(S_{kw}-S_{k'w})\right)=s_{cty,w}, \tag{19}$$

The terms multiplying $\nabla(S_{kw}-S_{k'w})$ are considered constant, yielding:

$$\phi\frac{\partial S_{kw}}{\partial t}+\nabla\cdot(S_{kw}\mathbf{u}_w)+0.5n_\kappa S_{k'w}\mathbf{n_{ij}}\cdot\underline{\underline{\sigma}}^{-1}_{k'w_{ij}}\cdot\mathbf{n_{ij}}\frac{|v^*_{w'_i}|\,l(S_{k'w_i}-S_{wirr})^{(-n_\kappa-1)}}{P_{sc}(1-S_{wirr})^{-n_\kappa}}\Delta(S_{kw}-S_{k'w})=s_{cty,w}, \tag{20}$$

In this way, an extra term is obtained; this is effectively a diffusion term, which is then discretised as normal. This same procedure is performed for the non-wetting phase.

In our experience, an exponent $n_\kappa = 2.0$ in Eq. 15 provides the best performance when physical capillary pressure is present. When capillary pressure is not present $n_\kappa = 1.0$ is preferable as it reduces the non-linearity of the VAD term. These are the values used in the numerical experiments reported here. Also, to avoid division by zero, the term

$$\left(\frac{S_{w_i}-S_{wirr}}{1-S_{wirr}}\right)^{-n_\kappa} \tag{21}$$

is modified to include a tolerance:

$$\left(\frac{S_{w_i}+S_{tol}-S_{wirr}}{1-S_{wirr}}\right)^{-n_\kappa}, \tag{22}$$

where we choose here $S_{tol} = 10^{-3}$. Fig. 1 shows the potential value of VAD for different saturations with $S_{wirr} = 0$. It can be seen that the potential value of VAD is very high for low saturation values and, therefore, at a shock-front, and very low for medium to high saturation values behind a shock-front.

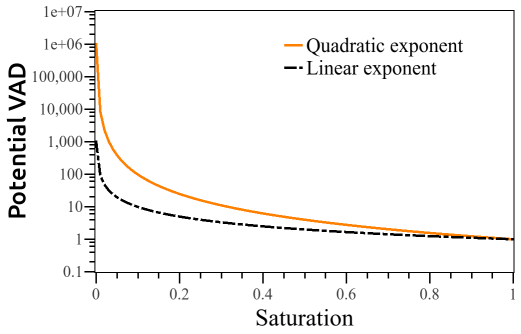


Figure 1: Potential value of VAD for different saturations considering the rest of the terms to be one and $S_{wirr} = 0$.

3.3. Vanishing Artificial Diffusion to guide the non-linear solver to a correct solution

In porous media flow, there are four main non-linearities that strongly affect the performance of the non-linear solver: steep saturation gradients ('shock fronts'), gravity, capillary pressure and phase change (Li and Tchelepi (2015b)). For simplicity in explaining the behaviour of VAD, we focus here on shock fronts only. When iteratively solving a linear or non-linear system, an initial solution estimate that is close to the final solution significantly reduces the time required by the solver to achieve convergence. The concept of VAD is to guide the non-linear solver towards the correct physical solution by constantly moving the "goal" of the non-linear solver.

Fig. 2 shows the results obtained using different levels of artificial diffusion without the vanishing term. It can be seen that the higher the artificial diffusion introduced, the further away the obtained solution is from the actual solution. From Fig. 2, one can see that using an initial $P_{sc} = 10$, the non-linear solver needs to modify the solution substantially to reach the final correct solution. Using a value of $P_{sc} = 100$, the effort required by the non-linear solver is drastically reduced as the initial solution is much closer to the final correct solution. However, the shock-front is less sharp, reducing the complexity of the system that the non-linear solver has to resolve.

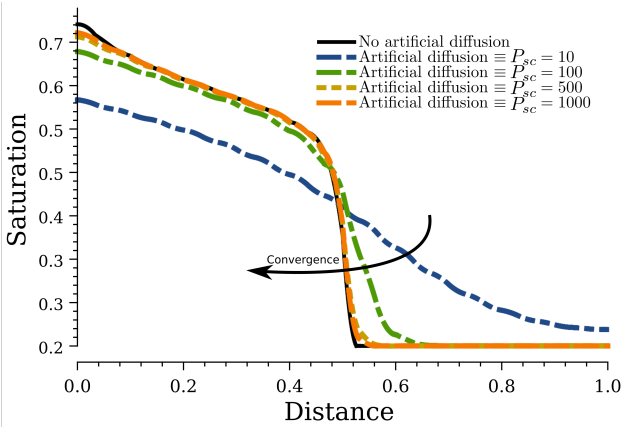


Figure 2: 1D solutions using different levels of classical artificial diffusion, that would be equivalent to the corresponding P_{sc} values if the system were to converge without the vanishing term. The black line is the result not using artificial diffusion. The blue, green, yellow and orange lines are the results with classical artificial diffusion equivalent to $P_{sc} = 10$, 100, 500 and 1000 respectively.

3.4. Monotonicity results when using high-order methods and Vanishing Artificial Diffusion

As we show later, when using high-order methods/elements the saturation solution obtained using VAD can in some cases be non-monotonic. When using low-order elements with high-order methods to calculate fluxes, we have observed that for values of $P_{sc} \geq 100$, monotonic solutions are obtained if the first non-linear iteration uses upwinding to calculate the fluxes instead of high-order methods. When using high-order elements and methods, it is also necessary to use a robust non-linear solver such as the one described in Salinas et al. (2017a). Values of $P_{sc} \geq 100$ are again required. Hence, non-linearity in the solutions can be easily removed for the recommended value of $P_{sc} \sim 100$.

4. Numerical experiments

The non-linear solver used is described in (Salinas et al. (2017a)). The convergence criteria used here are, unless otherwise stated, that the relative mass conservation of the system within a time-step has to be below 10^{-3} and the infinite norm of the saturation difference between two consecutive non-

linear iterations has to be below 10^{-2}. A maximum of 25 non-linear iterations per time-level is imposed.

To calculate the relative permeability and capillary pressure, the Brooks-Corey models are used (Brooks and Corey (1964)). The relative permeability is defined as:

$$k_{rw}\left(S_w\right) = \left(\frac{S_w - S_{wirr}}{1 - S_{wirr} - S_{nwr}}\right)^{n_w}, \tag{23}$$

$$k_{rnw}\left(S_{nw}\right) = \left(\frac{S_{nw} - S_{nwr}}{1 - S_{wirr} - S_{nwr}}\right)^{n_{nw}}, \tag{24}$$

where S_{nwr} is the irreducible non-wetting phase saturation and n_w and n_{nw} are the exponents for the wetting and non-wetting phases, respectively. Unless otherwise stated, the exponents of the relative permeability model used are $n_w = n_{nw} = 2$. For the capillary pressure the model used is the Brooks-Corey model (Brooks and Corey (1964)):

$$p_c(S_w) = P_{entry}\left(\frac{S_w + S_{tol} - S_{wirr}}{1 - S_{nwr} - S_{wirr}}\right)^{-n_{pc}}, \tag{25}$$

where P_{entry} is the entry pressure and n_{pc} is the exponent, set to $n_{pc} = 0.5$,. For simplicity, homogeneous capillary pressure is considered in the tests, but the method is not limited to this. The porosity is the same and homogeneous for all the test cases and is set to $\phi = 0.2$. All the remaining parameters for the three test cases are provided in Table 1. In test cases 4.1 and 4.4, the

	M^0	$\mathbf{K}_1$	$\mathbf{K}_2$	S_{wirr}	S_{nwr}	$\Delta\rho$	P_{entry}	u_{in}	length	# ele	Δt
4.1	1	1.0	N/A	0.2	0.3	0	N/A	0.2	1.0	240	0.01
4.2	10	1.0	N/A	0.2	0.3	0.289	0.1	N/A	0.3	160	0.025
4.3	1	1.0	0.001	0.2	0.3	0.289	N/A	N/A	1.0	720	1.0
4.4	10	10^{-12}	10^{-15}	0.2	0.2	289	10^5	N/A	220	25332	21600

Table 1: Model set-up for the test cases 4.1 – 4.4; M^0 is the viscosity contrast between the phases and u_{in} is the inlet velocity. For test case 4.3 the permeability, porosity and the relative permeability exponents are defined in subsection 4.3

domain is initially saturated with the non-wetting phase at $(1 - S_{wirr})$. Test cases 4.1, 4.2 and 4.3 are dimensionless. For 4.4, S.I. units are used.

4.1. 1D immiscible displacement

The formulation presented is tested against the semi-analytical solution of the Buckley-Leverett test case (Buckley and Leverett (1942)). Here, a

non-wetting phase is displaced by a wetting phase through a homogeneous domain (Fig. 3). This test case is used to study the effect of using different values of artificial vanishing capillary pressure (P_{sc}) for different Courant numbers, discretisations and convergence criteria of the non-linear solver.

In this test, only the vanishing artificial capillary pressure is used to stabilise the non-linear system. The time-step size is set to 10^{-2}, different Courant numbers are tested by using different meshes or element pairs, and the Courant number ranges from 0.5 to 2.5.

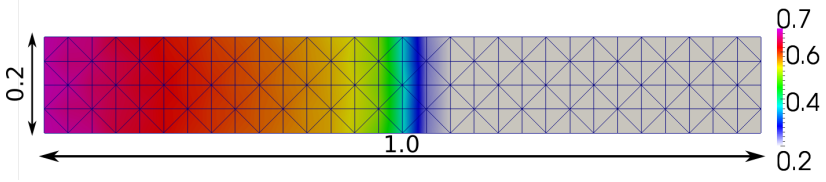


Figure 3: Domain dimensions together with the structured mesh used and the saturation profile at dimensionless time $t = 0.2$.

Fig. 4 shows the saturation profile for different values of P_{sc} and element pairs. The reference case is the same numerical experiment without VAD but with all the stabilisation techniques presented in (Salinas et al. (2017a)) and provides the best possible solution for the given mesh and discretisation. Fig. 4 shows the saturation profile for the $P_0DGP_1(CV)$ element pair. The result with $P_{sc} = 100$ is in good agreement with the semi-analytical result. Using $P_{sc} = 10$ provides a result with some oscillations, while $P_{sc} = \infty$ yields a good result but at the expense of more non-linear iterations (Table 2). The non-monotonic results appear when using a high-order advection scheme, or when the non-linear solver does not achieve convergence. We tested this same test case with upwinding and the results were always monotonic. As discussed earlier, to remove the non-monotonicity, an initial non-linear iteration using upwinding can be performed before employing the high-order scheme for the remaining non-linear iterations. This is sufficient to provide monotonic results with values of $P_{sc} \geq 100$. Lower values of P_{sc} are not desirable in any case, as they do not reduce the computational cost of the non-linear solver while providing accurate results.

Fig. 4 (B) shows the saturation profile for the higher-order $P_1DGP_2(CV)$ element pair. The result with $P_{sc} = 100$ is again in good agreement with the semi-analytical result. Simulations with $P_{sc} = 1000$ were carried out,

showing no benefit when compared with the results using $P_{sc} = 100$. Using $P_{sc} = 10$ provides a result with some oscillations, while $P_{sc} = \infty$ also provides a result with oscillations, because the non-linear solver does not converge. Note that the $P_{sc} = 100$ results also show some non-monotonicity, despite the use of upwinding for the first velocity iteration. However, by using commonly employed stabilisation techniques in addition to VAD (as used by Salinas et al. (2017a)), we obtain monotonic results (see Fig. 4 (B) $P_1DGP_2(CV)\, P_{sc} = 100^*$ plot). Monotonicity is always observed in numerical experiments with $P_{sc} \geq 100$ where stabilisation methods are used along with upwinding for the initial velocity iteration.

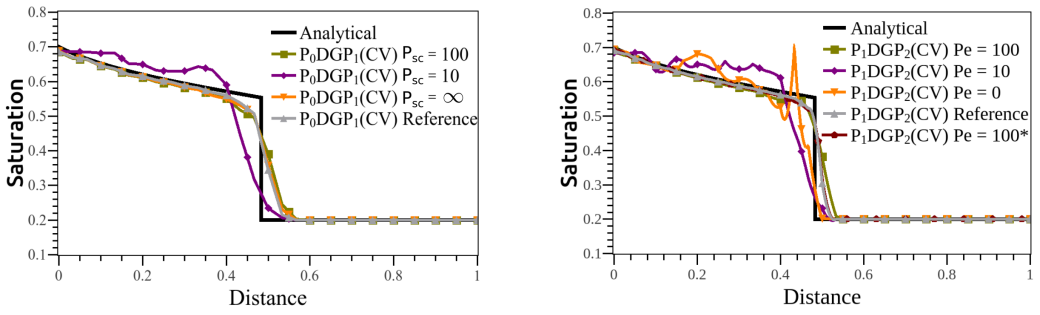


Figure 4: Saturation as a function of distance along the solution domain, comparing numerical solutions against the semi-analytical solution for the Buckley-Leverett problem. Numerical results obtained using different values of P_{sc} are shown; note that $P_{sc} = \infty$ means that no VAD is used. (A) Results using the $P_0DGP_1(CV)$ element pair; (B) results using the the $P_1DGP_2(CV)$ element pair. The result $P_1DGP_2(CV)\, P_{sc} = 100^*$ ws obtained using the stabilisation techniques presented in Salinas et al. (2017a) and shows monotonic results.

Table 2 shows the number of non-linear iterations together with the L_1 error for the results shown in Fig. 4. $P_{sc} = 100$ yields the best results, reducing the number of non-linear iterations and the error more than the other options. For the $P_1DGP_2(CV)$, element pair, the case with $P_{sc} = 100$ requires many more iterations than the case with $P_{sc} = 10$, but the error in the latter is higher, and therefore, $P_{sc} = 100$ is still preferable.

Table 3 shows the number of non-linear iterations and the L_1 error on a finer mesh (960 elements) when performing 20 time-steps and using the $P_0DGP_1(CV)$ element pair. Again $P_{sc} = 100$ provides the best combination

Element pair	P_{sc}	# non-linear iterations	L_1 error $\times 10^{-2}$
$P_0DGP_1(CV)$	100	85	1.59
$P_0DGP_1(CV)$	10	93	2.52
$P_0DGP_1(CV)$	∞	201	1.47
$P_1DGP_2(CV)$	100	168	1.32
$P_1DGP_2(CV)$	10	83	2.44
$P_1DGP_2(CV)$	∞	N/A	1.71

Table 2: Total number of non-linear iterations to perform 20 time-steps and the final error compared with the semi-analytical solution for the Buckley-Leverett problem using different values of P_{sc} and element pairs.

of performance and error reduction.

P_{sc}	# non-linear iterations	L_1 error $\times 10^{-2}$
100	163	1.01
10	78	2.53
∞	N/A	2.16

Table 3: Total number of non-linear iterations to perform 20 time-steps and the final error compared with the semi-analytical solution for the Buckley-Leverett problem, using different values of P_{sc} and one mesh refinement yielding a mesh with 960 elements.

It is important to note that, since the VAD used depends on the difference between the values of saturation of the last two non-linear iterations, this effectively means that the error of the results and the appropriate value of P_{sc} does depend on the convergence criteria used. When the system converges, the difference between the values of saturation of the last two non-linear iterations is small and of the order 10^{-2} or 10^{-3}; however, the VAD introduced may be larger (1) resulting in a residual artificial diffusion that persists in the final result. This residual VAD could, in principle, be completely removed by performing some extra non-linear iterations with no VAD. However, we have observed that the extra computational cost is very high; more than one non-linear iteration is typically required, and the benefit is marginal.

Fig. 5 shows shows the saturation profile for the $P_0DGP_1(CV)$ element pair, using three different convergence criteria and two different values of P_{sc}. It can be seen that for a very strict convergence criterion, $P_{sc} = 10$ provides very good results and there is virtually no difference compared to using $P_{sc} = 100$ (Table 4); moreover, the results are monotonic regardless

of the VAD used. However, for more relaxed convergence criteria this is no longer true and the cases using $P_{sc} = 100$ provide better results. Therefore, a value of $P_{sc} = 100$ is preferable. Table 4 shows that, depending on the convergence and P_{sc} number used, the number of non-linear iterations and solution accuracy obtained may vary. However, $P_{sc} = 100$ provides the best combination of fewer non-linear iterations and more accurate results.

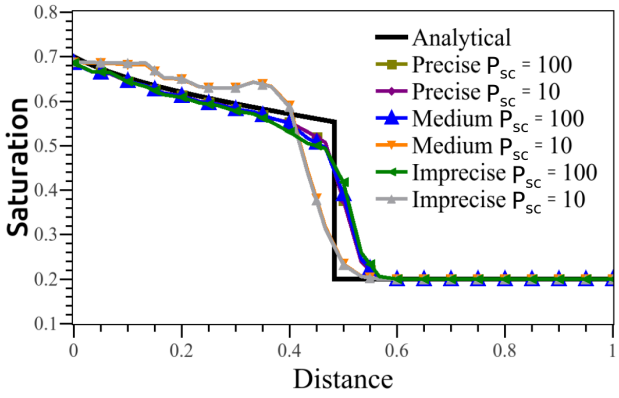


Figure 5: Saturation as a function of distance along the solution domain, comparing numerical solutions against the semi-analytical solution for the Buckley-Leverett problem. Numerical results are shown for different convergence criteria and different values of P_{sc}. 'Precise' denotes a convergence criterion where the infinite norm of the difference of the saturation between non-linear iterations has to be below 10^{-5}; 'medium' has the norm below 10^{-2} and 'imprecise' has it below 3×10^{-2}.

4.2. Counter-current flow driven by gravity and capillary forces

We now test the ability of the method to simulate gravity-capillary equilibrium in a situation where the capillary forces are dominant; we explore again the effect of the VAD (P_{sc}) for different discretisations and Courant numbers (ranging from 1.5 to 17). The initial condition of the model has a more dense wetting phase above a less dense non-wetting phase, so flow driven by both gravity and capillary forces occurs to reach the equilibrium state. This equilibration step is required to initialize any reservoir simulation model that includes (drainage) capillary pressure. We test the accuracy with which the simulation reaches equilibrium by comparing the wetting phase saturation as a function of height against a simple analytic solution where

Convergence level	P_{sc}	# non-linear iterations	L_1 error $\times 10^{-2}$
Precise	100	60	1.46
Precise	10	98	1.46
Medium	100	4	1.59
Medium	10	4	2.52
Imprecise	100	4	1.75
Imprecise	10	2	2.58

Table 4: L_1 error and number of non-linear iterations required to achieve convergence in the final time-step of the Buckley-Leverett problem ($t = 0.2$) using different convergence criteria of the non-linear solver and different values of P_{sc}. Notice that in the 'precise' case, the number of required non-linear iterations is much higher than in the other two cases; this is because the requested precision is 3 orders of magnitude smaller than the 'medium' case and a non-linear solver with linear convergence is being used.

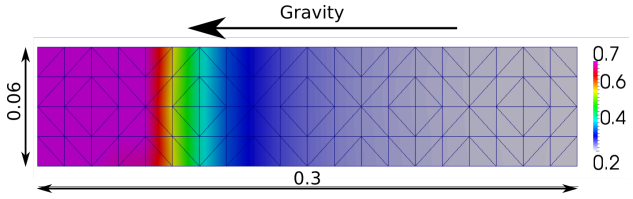


Figure 6: Domain dimensions together with the structured mesh used and the saturation profile at dimensionless time $t = 0.5$.

h is the height above datum, taken here to be the level at which capillary forces are zero. The analytical solution is defined as:

$$p_c(S_w) = (\rho_w - \rho_{nw})\mathbf{g}h \tag{26}$$

Fig. 7 shows the comparison of the water saturation profile obtained numerically for different values of P_{sc} and using two different element pairs ($P_0DGP_1(CV)$ and $P_1DGP_2(CV)$). The maximum Courant number is 17. It can be seen that the results with $P_{sc} = 100$ are in good agreement with the analytical solution and the reference numerical solution. However, for large VAD i.e. $P_{sc} = 1$ and $P_{sc} = 10$, the solution is wrong with obvious diffusive effects.

The number of non-linear iterations in order to perform 20 time-steps, together with the L_1 error are in Table 5. The results confirm that the best option is to use $P_{sc} = 100$, as it reduces the number of non-linear iterations whilst also keeping the error low. For $P_1DGP_2(CV)$ the results

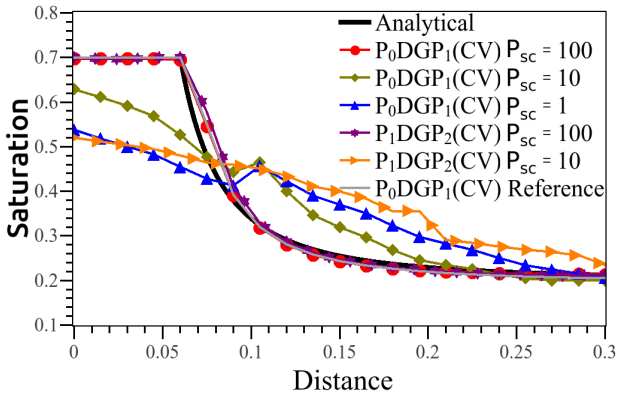


Figure 7: Saturation as a function of distance along the solution domain, comparing numerical solutions against the analytical solution for gravity-capillary equilibrium. Only converged numerical results are presented. The reference numerical solution was obtained without VAD.

are less accurate because the Courant number is higher than in the case with $P_0DGP_1(CV)$. To run the reference simulation without VAD (see Fig. 7), the time-step size needed to be reduced by 3 orders of magnitude, totalling 41246 non-linear iterations. Therefore, we can conclude that VAD is extremely useful to help the non-linear solver achieve convergence when capillary pressure plays a key role in the numerical experiment.

Element pair	P_{sc}	# non-linear iterations	L_1 error $\times 10^{-2}$
$P_0DGP_1(CV)$	100	50	1.65
$P_0DGP_1(CV)$	10	48	4.49
$P_0DGP_1(CV)$	1	199	6.89
$P_1DGP_2(CV)$	100	109	1.90
$P_1DGP_2(CV)$	10	460	9.17
$P_1DGP_2(CV)$	1	413	18.9

Table 5: Total number of non-linear iterations to perform 20 time-steps and the final error compared with the analytical solution for gravity-capillary equilibrium using different values of P_{sc} and element pairs.

4.3. Flow driven by gravity in a heterogeneous domain

For this test case we study the performance of VAD when flow is driven only by gravity. Initially, the domain is homogeneously filled by two fluid phases (above the immobile fraction); then, due to gravity, the phases segregate. This is a very challenging case due to the appearance of many shock-fronts moving with counter-current flow. Moreover, to explore a wider range of parameters, the domain is heterogeneous with different relative permeability curves, porosities and permeabilities. Fig. 8 (A) shows the mesh used and the regions with different material properties. For this test case only solutions with the optimal P_{sc} (i.e. $P_{sc} = 100$) and no VAD are tested.

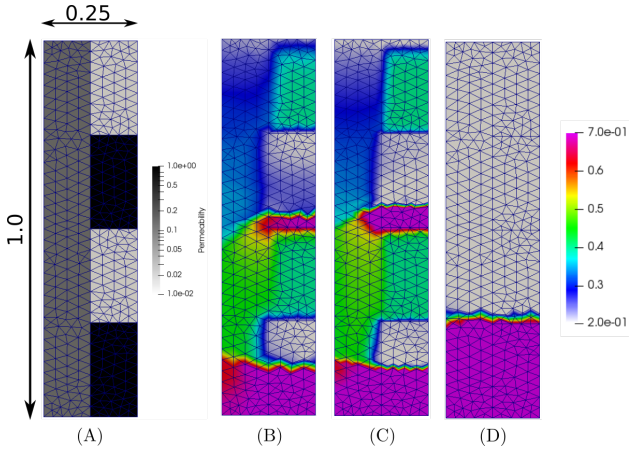


Figure 8: (A) Domain dimensions and mesh used. The dark, gray and white regions have a permeability of 1, 0.05 and 0.001, porosity of 0.3, 0.2 and 0.1, respectively. The dark and grey regions have quadratic relative permeability curves, while the white has linear relative permeability curves.(B) Saturation of the wetting phase after two time-steps using the $P_0DGP_1(CV)$ element pair. (C) Saturation of the wetting phase after at the same time level as (B) using the $P_1DGP_2(CV)$ element pair. (D) Saturation of the wetting phase after reaching equilibrium.

Fig. 8 (B-C) and Fig. 8 (D) show the saturation of the wetting phase in the gravity dominated problem at dimensionless time 0.1 and after reaching equilibrium, respectively. It can be seen that many shock-fronts are created (two per region initially) and propagate through the domain to finally reach the equilibrium state shown in Fig. 8 (C).

Table 6 shows the number of non-linear iterations required to perform 10 and 20 time-steps for the $P_0DGP_1(CV)$ and the $P_1DGP_2(CV)$ element pairs

Element pair	P_{sc}	# non-linear iterations	Courant number
$P_0DGP_1(CV)$	100	152	308.54
$P_0DGP_1(CV)$	∞	N/A	488.34
$P_1DGP_2(CV)$	100	397	348.49
$P_1DGP_2(CV)$	∞	N/A	486.82

Table 6: Total number of non-linear iterations to perform 10 time-steps in the gravity dominated problem for the $P_0DGP_1(CV)$ element pair and 20 time-steps for the $P_1DGP_2(CV)$ element pair, and the maximum Courant number that appears during the simulations for different element pairs and P_{sc}.

respectively. For the $P_1DGP_2(CV)$ element pair, the time-step is halved to reduce the expected maximum Courant number. In both scenarios without VAD, the non-linear solver fails to achieve satisfactory convergence and therefore the results are incorrect. However, using VAD the results obtained are physically correct and the number of non-linear iterations is small considering the high Courant number and the difficulty of the numerical experiment. We conclude again that VAD is extremely useful to help the non-linear solver achieve convergence.

4.4. Faulted reservoir with contrasting permeability layers

In this final test case a more realistic heterogeneous domain is modelled (Fig. 9 (A)). There is no analytical solution available and the performance of difference values of P_{sc} are tested.

The domain is defined by a set of contrasting permeability layers (10^{-12}m2 and 10^{-15}m2) that have been offset by two generations of faults with differing dip and strike. The model was created using a surface-based modelling algorithm which creates geological models using NURBS (Non-Uniform Rational B-Splines) surfaces (Jacquemyn et al. (2019)). The mesh was created using an automated geometry-adaptive meshing workflow with the NURBS surfaces as input (Melnikova et al. (2016)).

In this experiment, the left boundary is open with an inlet pressure of $P = 10^7$ Pa and the right boundary is open with a defined pressure of $P = 2 \times 10^5$ Pa; the other boundaries are closed to flow. Water is introduced through the higher pressure boundary to displace oil through the lower pressure boundary. Initially, the model is saturated with oil, and water at the irreducible saturation. The simulation is run using the element pairs $P_0DGP_1(CV)$ and $P_1DGP_2(CV)$ with $P_{sc} = 100$ and $P_{sc} = \infty$ (i.e. $\kappa = 0$);

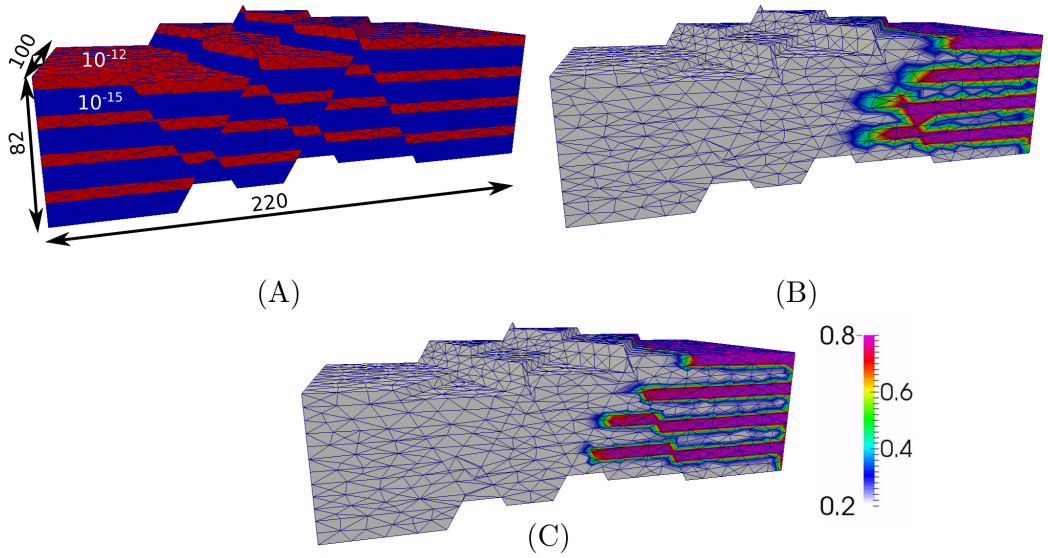


Figure 9: (A) Domain dimensions together with the mesh used and the permeability map. (B) Saturation profile after 5 days using the $P_0DGP_1(CV)$ element pair. (C) Saturation profile after 5 days using the $P_1DGP_2(CV)$ element pair.

the convergence criteria is the most relaxed i.e. the infinite norm has to be below 0.03. Also, the time-step size (Table 1) is reduced by a factor of eight for the element pair $P_1DGP_2(CV)$, to keep similar effective Courant numbers. Table 7 shows the number of non-linear iterations for these numerical experiments, together with the maximum Courant number in each simulation. It can be seen that the use of VAD significantly reduces the computational effort, allowing accurate solutions with larger Courant numbers. Moreover, in simulations without VAD, the maximum number of non-linear iterations was reached several times; thus convergence was not achieved and the solutions are not accurate.

5. Conclusions

An artificial diffusion that conserves mass, targets sharp shock-fronts and vanishes as the non-linear solver converges has been presented. Results show the efficiency of the method in reducing the number of non-linear iterations to achieve convergence under different scenarios. The addition of the presented VAD in the multiphase porous media flow equations significantly reduces the

Element pair	P_{sc}	# non-linear iterations	Courant number
$P_0DGP_1(CV)$	100	117	33.25
$P_0DGP_1(CV)$	∞	N/A	38.67
$P_1DGP_2(CV)$	100	767	149.30
$P_1DGP_2(CV)$	∞	N/A	173.82

Table 7: Total number of non-linear iterations to perform 20 time-steps in the fault model for the $P_0DGP_1(CV)$ element pair and 160 time-steps for the $P_1DGP_2(CV)$ element pair, and the maximum Courant number that appears during the simulations, for the different element pairs and P_{sc}.

non-linearity of the governing equations while minimising the effect of diffusion in the final results, leading to a faster and more stable non-linear solver. Different values of VAD have been studied, determined by a dimensionless Peclet-like number P_{sc} that provides a robust parameter to obtain optimal results. Results show that the optimal Peclet number requires the artificial diffusion forces introduced to be two orders of magnitude smaller than the viscous forces; this is to ensure that the final result is not affected by the diffusion introduced. Thus, the recommended value for VAD in a generic application is $P_{sc} = 100$ which, in combination with an initial use of upwinding to calculate the fluxes and a robust non-linear solver, will also guarantee monotonicity of the solution. The presented method is independent of the solver used and should equally work for Newton-Raphson methods.

Acknowledgements

Funding for Salinas from EPSRC (Smart-GeoWells grant EP/R005761/1) is gratefully acknowledged. Prof. Pain thanks the support from "Multi-scale Exploration of MultiPhase Physics In FlowS (MEMPHIS)" and "Investigation of the safe removal of fuel debris: multi-physics simulation". No data was generated in the course of this work. For further information, please contact the corresponding author at (pablo.salinas@imperial.ac.uk), the AMCG Group (www.imperial.ac.uk/earth-science/research/research-groups/amcg/) or the NORMS group (www.imperial.ac.uk/earth-science/research/research-groups/norms) as required.

References

Abushaikha, A., Blunt, M., Gosselin, O., Pain, C., Jackson, M. D., 2015. Interface control volume finite element method for modelling multi-phase fluid flow in highly heterogeneous and fractured reservoirs. Journal of Computational Physics, 41 – 61.

Abushaikha, A. S., Voskov, D. V., Tchelepi, H. A., 2017. Fully implicit mixed-hybrid finite-element discretization for general purpose subsurface reservoir simulation. Journal of Computational Physics 346, 514 – 538. URL http://www.sciencedirect.com/science/article/pii/S0021999117304874

Anderson, D. G., 1965. Iterative procedures for nonlinear integral equations. J. Assoc. Comput. Machinery 12, 547 – 560.

Aziz, K., Settari, A., 1979. Petroleum Reservoir Simulation. Applied Science Publishers, London.

Brenner, K., Cances, C., 2017. Improving newton s method performance by parametrization: The case of the richards equation. SIAM Journal on Numerical Analysis 55 (4), 1760 – 1785.

Brooks, R. H., Corey, A. T., 1964. Hydraulic properties of porous media. Colorado state university.

Buckley, S., Leverett, M., 1942. Mechanism of fluid displacements in sands. Transactions of the AIME (146), 107–116.

Cogswell, D. A., Szulczewski, M. L., 2017. Simulation of incompressible two-phase flow in porous media with large timesteps. Journal of Computational Physics 345, 856 – 865.

Debbabi, Y., Jackson, M. D., Hampson, G. J., Fitch, P. J. R., Salinas, P., Mar 2017a. Viscous crossflow in layered porous media. Transport in Porous Media 117 (2), 281–309.

Debbabi, Y., Jackson, M. D., Hampson, G. J., Salinas, P., oct 2017b. Capillary Heterogeneity Trapping and Crossflow in Layered Porous Media. Transport in Porous Media 120 (1), 183–206.

Deveugle, P., Jackson, M. D., Hampson, G., Farrell, M., Sprague, A., Stewart, J., Calvert, C., 2011. Characterization of stratigraphic architecture and its impact on fluid flow in a fluvial-dominated deltaic reservoir analog: Upper cretaceous ferron sandstone member, utah. AAPG Bulletin 95, 693–727.

Durlofsky, L., 1993. A triangle based mixed finite element finite volume technique for modelling two-phase flow through porous media. Journal Computational Physics 105, 252–266.

Durlofsky, L., 1994. Accuracy of mixed and control volume finite element approximations to Darcy velocity and related quantities. Water Resources Research 30, 965–973.

Forsyth, P., 1991. A control volume finite element approach to napl groundwater contamination. SIAM Journal of Scientific and Statistical Computing 12, 1029–1057.

Fung, L., Hiebert, A., Nghiem, L., 1992. Reservoir simulation with control-volume finite element method. SPE Reservoir Engineering 7 (3), 349–357.

Geiger, S., Roberts, S., Matthai, S., Zoppou, C., A. Burri, A., 2004. Combining finite element and finite volume methods for efficient multiphase flow simulations in highly heterogeneous and structurally complex geologic media. Geofluids 4 (4), 284–299.

Gomes, J., Pavlidis, D., Salinas, P., Xie, Z., Percival, J., Melnikova, Y., Pain, C., Jackson, M. D., 2017. A force-balanced control volume finite element method for multiphase porous media flow modelling. Int. J. Numer. Meth. Fluids 83, 431–445.

Hamon, F. P., Mallison, B. T., Tchelepi, H. A., 2016. Implicit hybrid upwind scheme for coupled multiphase flow and transport with buoyancy. Computer Methods in Applied Mechanics and Engineering 311, 599 – 624.

Hamon, F. P., Tchelepi, H. A., Jun 2016. Ordering-based nonlinear solver for fully-implicit simulation of three-phase flow. Computational Geosciences 20 (3), 475–493.

Hilpert, M., Marsh, B., Geiser, P. A., 2016. The radiator-enhanced geothermal system: Benefits of emulating a natural hydrothermal system. In: Interpretation,4(4):SR35.

Jackson, M. D., Percival, J., Mostaghimi, P., Tollit, B., D. Pavlidis, C. P., Gomes, J., El-Sheikh, A., P. Salinas, A. M., Blunt, M., 2015. Reservoir modeling for flow simulation by use of surfaces, adaptive unstructured meshes, and an overlapping-control-volume finite-element method. SPE Reservoir Evaluation and Engineering 18.

Jacquemyn, C., Hampson, G. J., Jackson, M. D., 2019. Surface-based geological reservoir modelling using grid-free nurbs curves and surfaces. Mathematical Geosciences.

Jameson, A., 1995. Analysis and design of numerical schemes for gas dynamics, 1: artificial diffusion, upwind biasing, limiters and their effect on accuracy and multigrid convergence. Int. J. Comp. FluidDyn 4, 171–218.

Janković, I., Fiori, A., Dagan, G., 2006. Modeling flow and transport in highly heterogeneous three-dimensional aquifers: Ergodicity, Gaussianity, and anomalous behavior - 1. Conceptual issues and numerical simulations. Water Resources Research 42 (SUPPL.), 1–9.

Jenny, P., Tchelepi, H., Lee, S., 2009. Unconditionally convergent nonlinear solver for hyperbolic conservation laws with s-shaped flux functions. Journal of Computational Physics 228, 7497 – 7512.

Jiang, J., Tchelepi, H., 2018. Dissipation-based continuation method for multiphase flow in heterogeneous porous media. arXiv.

Kvashchuk, A., 2015. A robust implicit scheme for two-phase flow in porous media. Master's thesis, University of Bergen, Norway.

Kwok, F., Tchelepi, H., Nov. 2007. Potential-based reduced Newton algorithm for nonlinear multiphase flow in porous media. Journal of Computational Physics 227, 706–727.

Lee, S., Efendiev, Y., Tchelepi, H., 2015. Hybrid upwind discretization of nonlinear two-phase flow with gravity. Advances in Water Resources 82, 27 – 38.

Li, B., Tchelepi, H., 2015a. Numerical trust region newton solver for multiphase transport in porous media based on detailed nonlinear analysis. In: SPE 173267.

Li, B., Tchelepi, H. A., 2015b. Nonlinear analysis of multiphase transport in porous media in the presence of viscous, buoyancy, and capillary forces. Journal of Computational Physics 297, 104 – 131.

Lott, P., Walker, H., Woodward, C., Yang, U., 2012. An accelerated fixed-point iteration for solution of variably saturated flow. Advances in Water Resources 38, 92 – 101.

Matthai, S., Mezentsev, A., Belayneh, M., 2007. Finite element-node centered finite-volume two-phase flow experiments with fractured rock represented by unstructured hybrid element meshes. SPE 93341.

McWhorter, D. B., Sunada, D. K., 1990. Exact integral solutions for two-hase flow. Water Resources Research 26 (3), 399–413.

Melnikova, Y., Jacquemyn, C., Osman, H., Salinas, P., Gorman, G., Hampson, G., Jackson, M. D., 2016. Reservoir modelling using parametric surfaces and dynamically adaptive fully unstructured grids. In: ECMOR XV - 15th European Conference on the Mathematics of Oil Recovery.

Mostaghimi, P., Percival, J., Pavlidis, D., Ferrier, R., Gomes, J., Gorman, G., Jackson, M. D., Neethling, S., Pain, C., 2015. Anisotropic mesh adaptivity and control volume finite element methods for nucmerical simulation of multiphase flow in porous media. Mathematical Geoscience 347, 673–676.

Natvig, J. R., Lie, K., 2008. Fast computation of multiphase flow in porous media by implicit discontinuous galerkin schemes with optimal ordering of elements. Journal of Computational physics.

Nooruddin, H. A., Blunt, M. J., 2016. Analytical and numerical investigations of spontaneous imbibition in porous media. Water Resources Research 52 (9), 7284–7310.

Pavlidis, D., Xie, Z., Percival, J., Gomes, J., Pain, C., Matar, O., 2014. Two- and three-phase horizontal slug flow modelling using an interface-capturing compositional approach. International Journal for Multiphase Flow 67, 85–91.

Quarteroni, A., Valli, A., 2009. Numerical Approximation of Partial Differential Equations.

Salinas, P., Pavlidis, D., Xie, Z., Adam, A., Pain, C. C., Jackson, M. D., 2017a. Improving the convergence behaviour of a fixed-point-iteration solver for multiphase flow in porous media. International Journal for Numerical Methods in Fluids 84 (8), 466 – 476.

Salinas, P., Pavlidis, D., Xie, Z., Jacquemyn, C., Melnikova, Y., Pain, C. C., Jackson, M. D., 2017b. Improving the robustness of the control volume finite element method with application to multiphase porous media flow. International Journal for Numerical Methods in Fluids 85, 235–246.

Schmid, K., Geiger, S., Sorbie, K., 2013. Higher order fefv method on unstructured grids for transport and two-phase flow with variable viscosity in heterogeneous porous media. Journal of Computational Physics 241 (0), 416 – 444.

Schmid, K. S., Geiger, S., 2013. Universal scaling of spontaneous imbibition for arbitrary petrophysical properties: Water-wet and mixed-wet states and Handy's conjecture. Journal of Petroleum Science and Engineering 101 (January), 44–61.

Solano, J. M. S., Jackson, M. D., Sparks, R. S. J., Blundy, J., 2014. Evolution of major and trace element composition during melt migration through crystalline mush: Implications for chemical differentiation in the crust. American journal of science 314, 895–939.

Soltanian, M. R., Amooie, M. A., Cole, D. R., Graham, D. E., Hosseini, S. A., Hovorka, S., Pfiffner, S. M., Phelps, T. J., Moortgat, J., 2016. Simulating the cranfield geological carbon sequestration project with high-resolution static models and an accurate equation of state. International Journal of Greenhouse Gas Control 54 (Part 1), 282 – 296.

Tchelepi, H. A., Jenny, P., Lee, S. H., Wolfsteiner, C., 2007. Adaptive Multiscale Finite-Volume Framework for Reservoir Simulation. SPE Journal 12 (02), 188–195.

Wheeler, M., Yotov, I., 2006. A multipoint flux mixed finite element method. SIAM. J. Numer. Anal. 44, 2082–2106.

Xie, Z., Pavlidis, D., Salinas, P., Percival, J., Pain, C., Matar, O., 2016. A balanced-force control volume finite element method for interfacial flows with surface tension using adaptive anisotropic unstructured meshes. Computers and Fluids 138, 38–50.

Younis, R., Tchelepi, H. A., Aziz, K., 2010. Adaptively localized continuation-newton method–nonlinear solvers that converge all the time. In: SPE Reservoir Simulation Symposium.